American Mineralogist, Volume 92, pages 648–654, 2007

Rhombohedral (9R) and hexagonal (6H) perovskites in barium silicates under high pressure

HITOSHI YUSA,[1,*] NAGAYOSHI SATA,[2] AND YASUO OHISHI [3]

[1]Advanced Nano Materials Laboratory, National Institute for Materials Science, 1-1 Namiki, Tsukuba, 305-0044, Ibaraki, Japan
[2]Institute for Frontier Research on Earth Evolution, Japan Agency for Marine-Earth Science and Technology, 2-15, Natsushima-cho, Yokosuka, 237-0061, Kanagawa, Japan
[3]Japan Synchrotron Radiation Research Institute, 1-1-1 Kouto, Sayo-cho, 679-5198, Hyogo, Japan

ABSTRACT

Rhombohedral (9R) and hexagonal (6H) perovskites in $BaSiO_3$ were observed by using in-situ X-ray diffraction methods in high-pressure conditions. The 9R perovskite was found after successive laser heating at 27.9 GPa, and the 6H phase was identified at 48.5 GPa after laser annealing. No intermediate phase between the 9R and 6H phases was found in the pressure range between 27.9 and 48.5 GPa. These phases could not be recovered during decompression at room temperature and became amorphous at ambient pressure. The 9R and 6H structures are characterized by the periodicity of the stacking sequence of edge- and corner-sharing SiO_6 octahedra. In terms of the length of the O-O distance, the face-sharing SiO_6 octahedron in $BaSiO_3$ perovskite is the most distorted among oxide hexagonal perovskites.

Keywords: Perovskite, high pressure, barium silicate, Rietveld method

INTRODUCTION

Silicate perovskites of the form $A^{2+}SiO_3$ are probably in significant abundance in the Earth's interior. In particular, silicate perovskites bearing Mg^{2+} and Ca^{2+} have attracted much attention because of their abundance in the lower mantle. Except for a minor tetragonal modification of $CaSiO_3$ peovskite (Shim et al. 2002), only cubic and orthorhombic forms of silicate perovskites have been discovered. Recently, the presence of hexagonal perovskite (6H-$BaTiO_3$ type) was found in strontium silicates at 35 GPa (Yusa et al. 2005), where Sr^{2+} takes the place of the A^{2+} cation. From the crystallographic aspect, the symmetry of such perovskites is associated with the ionic radii of divalent cations. The tolerance factor, $t = (r_A + r_O)/\sqrt{2}(r_{Si} + r_O)$, where r denotes the ionic radii of each element, has been viewed as an indicator of this association. Perovskite with a cubic structure has a tolerance factor close to 1.0 (e.g., $CaSiO_3$: $t = 0.99$), and hexagonal perovskite in $SrSiO_3$ has a value greater than unity ($t = 1.04$). In light of the very large tolerance factor ($t = 1.11$) of $BaSiO_3$, we decided to explore the systematics of the phase sequence of $A^{2+}SiO_3$.

The high-pressure transformation of $BaSiO_3$ was reported by Shimizu et al. (1970). By analyzing the X-ray diffraction pattern of the recovered products, they recognized a new phase ($BaSiO_3$ II) appearing from 4.3 to 12.0 GPa at 840–1400 °C. However, they were not able to determine the crystal structure. No in-situ experiment has been done on $BaSiO_3$ under high pressure. It is known that $CaSiO_3$ and $SrSiO_3$ perovskite cannot be recovered at ambient pressure due to amorphization during decompression. Hence, we tried to conduct in-situ X-ray diffraction experiments at pressures up to 53 GPa to examine the high-pressure phase of $BaSiO_3$.

* E-mail: yusa.hitoshi@nims.go.jp

EXPERIMENTAL PROCEDURES

The starting sample of $BaSiO_3$ was prepared from an equimolar mixture of $BaCO_3$ and silicic acid ($SiO_2 \cdot 11\%H_2O$). The grinding mixture was heated in a platinum crucible that was kept in an electrical furnace at 1623 K for 18 h. The structure was identified by X-ray diffraction methods as a structure of $BaSiO_3$ (h) (Grosse and Tillmanns 1974a), which is the same as the structure of high-temperature $BaGeO_3$ (Hilmer 1962). The sample was mixed with a small amount of platinum (less than 0.01 wt%) and put into a hole (0.1–0.15 mm in diameter) in a rhenium gasket, where it was compressed without a pressure medium in a diamond anvil cell (DAC). A few small grains of ruby pressure marker were put in the sample. The in-situ X-ray diffraction experiments were done under high pressure at SPring-8 (Watanuki et al. 2001). The compressed sample was heated with the Nd:YLF laser at the beam line (BL-10XU). The focused beam (20 μm in diameter) scanned the whole sample area, usually for 30 minutes. The temperature was monitored by spectroscopic measurements of the radiation emitted from the sample during heating. An imaging plate (IP) and a charge-coupled detector (CCD) were used to detect the diffracted X-rays. The wavelength of the incident X-ray beam was tuned to 30 keV by using an Si(111) monochromater and was collimated to 20 μm in diameter at the sample position. A wide conical aperture of the tungsten carbide seats made it possible to collect Debye rings up to about 16–17° in 2θ. The Debye rings were converted with a computer program (Fit-2D; Hammersley 1997) into two- or one-dimensional X-ray profiles plotted as a function of 2θ. A ruby pressure scale (Mao et al. 1986) was used for the pressure determination.

RESULTS AND DISCUSSION

Hexagonal perovskite phases under high pressure

Table 1 summarizes the experimental conditions and the results of all the high *P-T* experiments. First, we set the target pressure to ca. 30 GPa, where the transition to hexagonal perovskite takes place in $SrSiO_3$. During compression to 33.0

0003-004X/07/0004–648$05.00/DOI: 10.2138/am.2007.2314

GPa at room temperature, the starting $BaSiO_3$ (h) (Fig. 1a) phase was transformed into an unknown crystalline phase (Fig. 1b), which is in contrast to the pressure-induced amorphous phase observed in $SrSiO_3$ and $CaSiO_3$. After laser heating at 1500–1700 K, sharp diffraction peaks emerged (Fig. 1c) and the pressure dropped to 27.9 GPa due to the volume contraction that occurs along with the phase transition. The diffraction pattern was apparently different from that of 6H perovskite ($P6_3/mmc$), which is associated with the high-pressure phase in $SrSiO_3$ (Yusa et al. 2005). Instead, the pattern was similar to that of the 9R $BaMnO_3$ perovskite ($R\bar{3}m$) (Boullay et al. 1997). The Rietveld analysis was performed using GSAS (Larson and Von Dreele 2004) even though small, untransformed peaks (2θ = 7.2°, 8.2°, 8.8°, 9.7°) were in the pattern because of the vertical temperature gradient in the laser heated DAC (Morishima and Yusa 1998). As shown in Figure 2, the 9R perovskite is a possible structure for the high-pressure phase. Table 2 lists the refined d-values of the 9R perovskite at 27.9 GPa. The lattice parameters were determined to be a = 5.3002 Å and c = 19.2351 Å. Table 3 lists the atomic coordinates of the structure as determined by the Rietveld analysis. The displacement parameters were fixed to the isotropic displacement parameter (U_{iso}) of the related phase, to avoid inappropriate convergence of U_{iso} in the calculation. The phase became completely amorphous upon pressure release to atmospheric pressure.

Second, higher pressure was applied to confirm the stability of the pressure field of the 9R perovskite. The sample was pressurized to 53.0 GPa and heated to 2700 K. The pressure after laser heating was decreased by 10%. Many sharp peaks appeared (Fig. 3b). The new diffraction pattern can be assigned to the 6H perovskite structure (Table 4). The refined lattice parameters at 48.5 GPa were a = 5.1125 Å and c = 12.3871 Å (R_w = 0.071). The atomic coordinates (Table 5) were obtained from the Rietveld analysis (Fig. 4). Similar to the case of the 9R perovskite, this phase could not be recovered and became amorphous at ambient pressure. It is interesting that the pressure-induced phase (Fig. 3a) is completely different from the diffraction pattern of the preheated phase at 33.0 GPa. The pattern is rather similar to

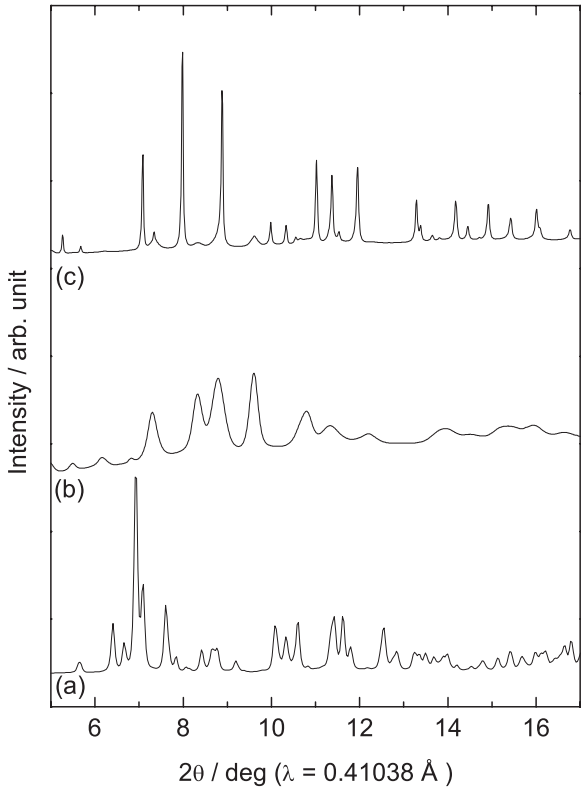

FIGURE 1. Integrated diffraction profiles of the IP: (**a**) Before compression; (**b**) at 33.0 GPa before laser heating; and (**c**) at 27.9 GPa after laser heating.

TABLE 1. Results of the high-pressure and high-temperature experiments on $BaSiO_3$

Run no.	P (GPa)*	T (K)†	Phase
BAS008	27.9	1500–1700	9R
BAS2012	48.5	1700–2700	6H
BAS3013	39.5	2000–2100	6H + 9R
BAS3022	33.3	2250–2300	9R
BAS3025	17.3	1800–2400	9R
BAS4010	16.5	1700–1800	Ba_2SiO_4 (K_2SO_4-type) + unknown
BAS5009	42.8	1800–2600	6H
BAS5012	26.4	1800–2600	9R

* After heating.
† Annealing temperature values.

TABLE 2. Refined X-ray powder diffraction data for 9R $BaSiO_3$ perovskite

h k l	d_{obs} (Å)	d_{ref} (Å)	$(d_{obs}/d_{ref}) - 1$
0 0 3		6.4150	
1 0 1	4.4664	4.4648	0.0004
1 0 2	4.1433	4.1425	0.0002
1 0 4	3.3217	3.3203	0.0004
0 0 6	3.2047	3.2058	–0.0004
1 0 5	2.9481	2.9484	–0.0001
1 1 0	2.6499	2.6501	–0.0001
1 1 3	2.4489	2.4492	–0.0001
1 0 7	2.3579	2.3577	0.0001
2 0 1	2.2788	2.2789	–0.0001
2 0 2	2.2318	2.2324	–0.0003
0 0 9	2.1368	2.1372	–0.0002
1 0 8		2.1299	
2 0 4	2.0710	2.0713	–0.0001
1 1 6	2.0421	2.0426	–0.0002
2 0 5	1.9709	1.9710	–0.0000
1 0 10	1.7734	1.7740	–0.0003
2 0 7	1.7607	1.7615	–0.0004
2 1 1	1.7271	1.7279	–0.0004
2 1 2	1.7058	1.7074	–0.0009
1 1 9	1.6625	1.6636	–0.0007
2 0 8		1.6602	
0 1 11		1.6341	
2 1 4	1.6312	1.6320	–0.0004
0 0 12	1.6019	1.6029	–0.0006
2 1 5	1.5808	1.5815	–0.0005
3 0 0	1.5292	1.5300	–0.0006

Notes: Rhombohedral, probable space group $R\bar{3}m$ (Z = 9), a = 5.3002 Å, c = 19.2351 Å, V = 467.97 Å^3 (R_w = 0.102) at 27.9 GPa.

TABLE 3. Refined atomic coordinates for $BaSiO_3$ 9R perovskite at 27.9 GPa

Atom	x	y	z	U_{iso}*
Ba1	0	0	0	0.0054†
Ba2	0	0	0.2127	0.0065†
Si1	0	0	0.5	0.0085‡
Si2	0	0	0.3696	0.0085‡
O1	0.5	0	0	0.0040†
O2	0.1416	–0.1416	0.5563	0.0043†

* Fixed values are used.
† $BaTiO_3$ hexagonal perovskite: Akimoto et al. (1994).
‡ $MgSiO_3$ orthorhombic perovskite: Horiuchi et al. (1987).

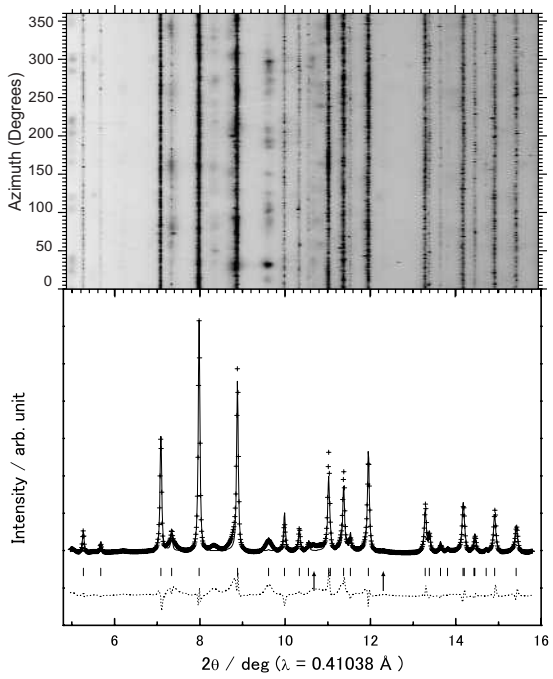

FIGURE 2. Powder X-ray diffraction pattern analyses using the Rietveld method (GSAS). Raw 2D image (azimuth vs. 2θ) is inserted for comparison. The observed pattern (crosses) is the same as in Figure 1c. The difference (dotted line) between the observed and fitted pattern (thin line) is also shown on the same scale. Background was subtracted. Tick marks represent the calculated positions of the diffraction peaks of the 9R perovskite phase. The reflections of platinum are indicated by arrows.

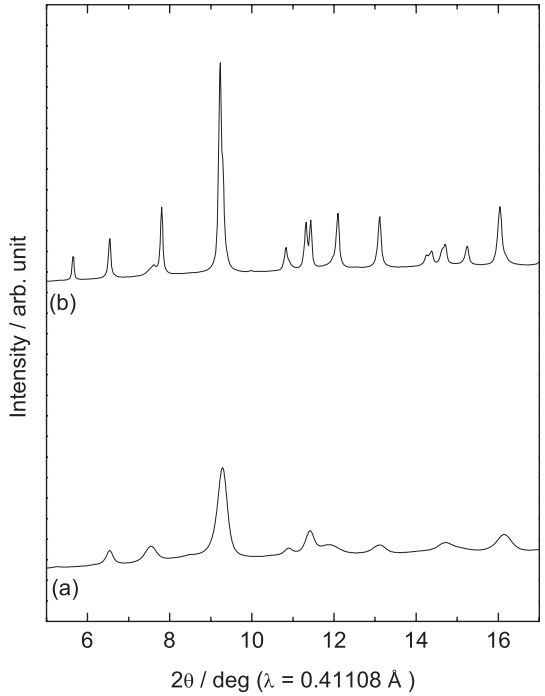

FIGURE 3. Integrated diffraction profiles of the IP: (**a**) at 53.0 GPa before laser heating; and (**b**) at 48.5 GPa after laser heating.

that of the 6H perovskite that formed after heating. However, attempts to index this pattern as the 6H phase was unsuccessful because of broad peaks and large errors.

Figures 5a and 5b show crystallographic drawings of 9R and 6H perovskites based on the present atomic coordinates. The SiO_6 octahedra and barium cations are illustrated along the *c*-axis to clarify their relationship with the stacking sequence. The 9R phase resembles the 6H phase in that the SiO_6 octahedra are periodically connected by face-sharing. The difference is in the periodicity of face- and corner-sharing of the SiO_6 octahedron. In the direction of the *c* axis, 9R perovskite exhibits a $(chh)_3$ sequence whereas 6H perovskite exhibits a $(cch)_2$ sequence, where c and h correspond to corner-and face-sharing octahedra, respectively, and the subscript means the number of repetitions of the sequence in parenthesis in the unit cell. It is known that such hexagonal polytypes in perovskite are found in a sequence from 2H to 3C. With increasing corner-sharing octahedra, 2H, 9R, 4H, and 6H perovskites appear in $BaRuO_3$ or $BaMnO_3$ (Longo and Kafalas 1968; Syono et al. 1969). In this hexagonal

TABLE 4. Refined X-ray powder diffraction data for 6H $BaSiO_3$ perovskite

h k l	d_{obs} (Å)	d_{ref} (Å)	$(d_{obs}/d_{ref}) - 1$
0 0 2		6.1935	
1 0 0		4.4275	
1 0 1	4.1721	4.1692	0.0007
1 0 2	3.6048	3.6019	0.0008
0 0 4	3.0991	3.0968	0.0008
1 0 3	3.0207	3.0197	0.0003
1 1 0	2.5559	2.5562	–0.0001
1 0 4	2.5361	2.5377	–0.0006
1 1 2	2.3634	2.3629	0.0002
2 0 0		2.2138	
2 0 1	2.1783	2.1792	–0.0004
1 0 5	2.1599	2.1620	–0.0010
2 0 2	2.0845	2.0846	–0.0001
0 0 6	2.0634	2.0645	–0.0005
1 1 4		1.9714	
2 0 3	1.9507	1.9510	–0.0002
1 0 6		1.8711	
2 0 4	1.8006	1.8009	–0.0002
2 1 0		1.6735	
2 1 1	1.6557	1.6584	–0.0016
2 0 5		1.6507	
1 0 7	1.6426	1.6432	–0.0004
2 1 2	1.6130	1.6155	–0.0016
1 1 6	1.6049	1.6061	–0.0008
2 1 3	1.5501	1.5509	–0.0005
0 0 8		1.5484	
2 0 6		1.5098	
3 0 0		1.4758	
2 1 4	1.4733	1.4722	0.0007
3 0 1		1.4655	
1 0 8	1.4584	1.4616	–0.0022
3 0 2		1.4357	

Notes: Hexagonal, probable space group $P6_3/mmc$ ($Z = 6$), $a = 5.1125$ Å, $c = 12.3871$ Å, $V = 280.39$ Å^3 ($R_w = 0.071$) at 48.5 GPa.

TABLE 5. Refined atomic coordinates for $BaSiO_3$ 6H perovskite at 48.5 GPa

Atom	*x*	*y*	*z*	U_{iso}*
Ba1	0	0	0.25	0.0054†
Ba2	0.3333	0.6667	0.0951	0.0065†
Si1	0	0	0	0.0085‡
Si2	0.3333	0.6667	0.8567	0.0085‡
O1	0.5279	0.0558	0.25	0.0040†
O2	0.8376	0.6751	0.0782	0.0043†

* Fixed values are used.
† $BaTiO_3$ hexagonal perovskite: Akimoto et al. (1994).
‡ $MgSiO_3$ orthorhombic perovskite: Horiuchi et al. (1987).

sequence, pressure increases the frequency of corner-sharing octahedra. This relation can be extended to cubic perovskite (3C), which only consists of corner-sharing octahedra. Actually, the cubic perovskite (3C) in $BaRuO_3$ is predicted to exist above 12 GPa (Longo and Kafalas 1968). On the basis of these systematics, we tried to find 2H, 4H, and 3C perovskite in $BaSiO_3$ by conducting additional experiments (Table 1). To confirm the existence of 4H perovskite, the sample was heated at 39.5 GPa, which is an intermediate pressure between those of 9R and 6H perovskites. However, this experiment only found the coexisting phases of 9R and 6H. We could not find any peaks from 4H perovskite in $BaSiO_3$. The volume difference between 9R and 6H was calculated to be 3.5%, comparable to the volume difference of 2.9% resulting from 9R to 6H via 4H perovskite in $BaMnO_3$. Subsequently, we gradually reduced the pressure and heated the sample repeatedly to survey the lower pressure phases. The reversal experiments (no. BAS3025) indicated that the 9R perovskite was stable down to at least 17.3 GPa. On the other hand, the newly compressed run (no. BAS4010) suggested that the phase decomposes into two phases at 16.5 GPa. One phase was assigned to K_2SO_4-type Ba_2SiO_4 (Grosse and Tillmanns 1974b), whereas the other phase could not be assigned to any known structure. Considering that AXO_3 compounds, such as $CaSiO_3$, $SrSiO_3$, and $BaGeO_3$, break down into A_2XO_4 and AX_2O_5 prior to their transition to perovskite (Angel 1997, Kojitani et al. 2005, Ozima et al. 1982), the possible stoichiometry of the unknown phase would be $BaSi_2O_5$ in the case of $BaSiO_3$. Further analysis would be necessary to determine the unknown phase. In the present experiments we could not find either 2H and 3C perovskite.

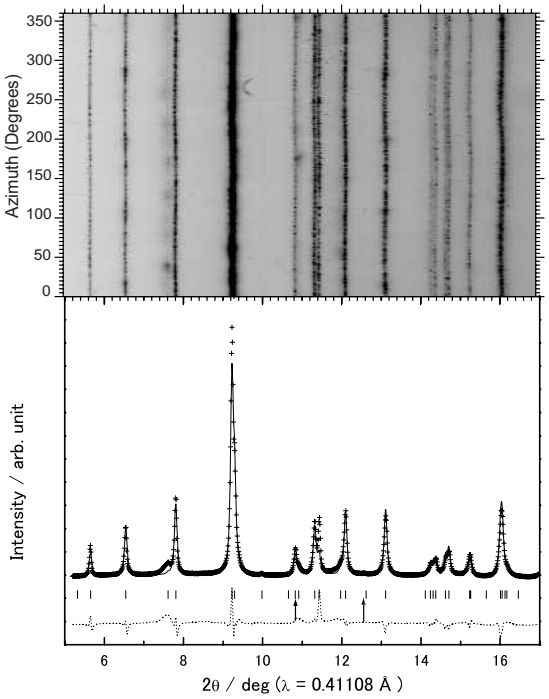

FIGURE 4. Powder X-ray diffraction pattern analyses using the Rietveld method (GSAS). Raw 2D image (azimuth vs. 2θ) is inserted for comparison. The observed pattern (crosses) is the same as in Figure 2b. The difference (dotted line) between the observed and fitted pattern (thin line) is also shown on the same scale. Background was subtracted. Tick marks represent the calculated positions of the diffraction peaks of the 6H perovskite phase. The reflections of platinum are indicated by arrows.

Structural stability during decompression

Both $CaSiO_3$ and $SrSiO_3$ perovskites exhibit amorphization when the pressure is completely released (Liu and Ringwood 1975, Yusa et al. 2005). In the case of $CaSiO_3$ perovskite, amorphization occurs very close to 1 atm. For example, Mao et al. (1989) performed DAC experiments showing that $CaSiO_3$ perovskite is stable down to a pressure of 0.1 MPa. Kanzaki et al. 1991 demonstrated partial quenchability from a product by using a large volume apparatus. It is suggested that quenchability is increased by substitution of Ti in $CaSiO_3$ perovskite. In a $CaSiO_3$–$CaTiO_3$ join, 83 mol% $CaSiO_3$, synthesized at 12.5 GPa and 1000 °C, can be quenched as cubic perovskite (Kubo

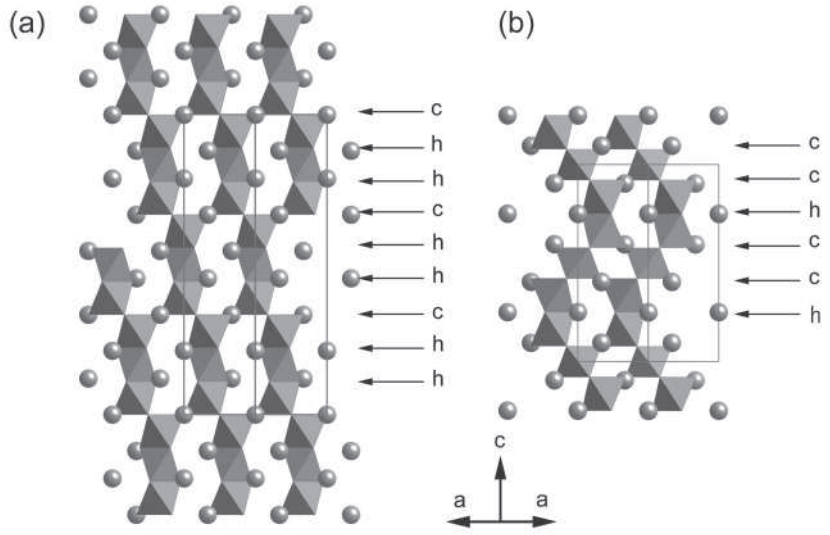

FIGURE 5. Projection of the hexagonal perovskite structures in $BaSiO_3$ along the *c* axis. (**a**) 9R phase. (**b**) 6H phase. The unit cell is indicated by the red lines; c and h denote corner sharing and face sharing of the SiO_6 octahedra, respectively.

et al. 1997). A similar situation might occur with a $BaTiO_3$–$BaSiO_3$ solid solution. Therefore, the quenchability of $BaSiO_3$ is significant for not only understanding the systematics of silicate perovskites, but also for searching for ferroelectrics along the $BaTiO_3$–$BaSiO_3$ join. For this reason, we examined the stability of hexagonal perovskites in $BaSiO_3$. First, half of the sample area was heated at 47.8 GPa to obtain 6H perovskite, and 9R perovskite was synthesized on the other half by heating after decompression to 33.0 GPa. After that, the diffraction patterns were measured at room temperature as the pressure decreased to ambient. The 6H perovskite began to decompose at 21.9 GPa (Fig. 6a), whereas the 9R perovskite was still present at 8.9 GPa (Fig. 6b). The 9R perovskite became amorphous at 4.8 GPa. At 1.8 GPa, both phases became completely amorphous.

Distortion of octahedron in hexagonal perovskites

When the tolerance factor is less than unity, as is the case with the $MgSiO_3$ perovskite, the SiO_6 octahedron tilts to make allowance for small divalent cations in the SiO_6 octahedral corner-sharing framework, in which the Mg-O bond lengths of the 12-fold site are no longer equal, but SiO_6 octahedron remains rigid (Horiuchi et al. 1987). Tilting in perovskites, where rotation does not disrupt the corner-sharing connectivity, has been discussed by many researchers (e.g., Glazer 1972). On the other hand, in the present study, perovskites bearing large divalent cations tend to adopt a SiO_6 face-sharing octahedral framework, which expands the cavities to accommodate larger cations. The octahedron itself is somewhat distorted because the Si^{4+} ions in face-sharing octahedra cause the oxygen anions to move closer to reduce Si-Si repulsion. Therefore, the O-O distance in the shared face is shorter than the distance associated with a shared corner. In contrast, the deviation of the Ba-O bond length from an ideal 12-fold site is small. These relations can be easily understood from the cuboctahedron of 9R and 6H perovskites illustrated in Figure 7. The bond lengths of 9R and 6H are listed in Table 6 and 7, respectively.

Several hexagonal perovskites are found in the other barium compounds consisting of XO_6 (X = Si, Ti, Mn, Rh, Ru, Cr) face-sharing octahedra There is a clear trend to indicate that the smaller X^{4+} ions have shorter O-O distances (Akimoto et al. 1994; Boullay et al. 1997; Chamberland and Anderson 1981; Hong and Sleight 1997; Chamberland 1982, 1983). To accept a large cation in the 12-fold site, the SiO_6 octahedron must undergo a large distortion due to small ionic radii of Si^{4+}. Therefore, O-O distances are a general indicator of the distortion of the XO_6 octahedron in $BaXO_3$ hexagonal perovskites.

Element partitioning experiments (Kato et al. 1988) indicated

TABLE 6. Interatomic distance of $BaSiO_3$ 9R perovskite at 27.9 GPa

Interatomic distance (Å)		
$Si1O_6$ octahedron		
O2-O2	3.38(4)	×3
O2-O2	2.25(4)	×6
O2-O2	2.53(4)	×6
Si1-O2	1.692(22)	×6
Si1-Si2	2.509(24)	×2
$Si2O_6$ octahedron		
O1-O2	3.537(25)	×3
O1-O2	2.558(21)	×6
O1-O1	2.6501(1)	×3
O2-O2	2.25(4)	×3
Si2-O1	1.681(10)	×3
Si2-O2	1.929(23)	×3
Si2-Si2	3.362(20)	×3
Ba-O cuboctahedron		
Ba1-O1	2.6501(1)	×6
Ba1-O2	2.758(22)	×6
Ba2-O2	2.641(24)	×3
Ba2-O2	2.6675(30)	×6
Ba2-O1	2.780(5)	×3

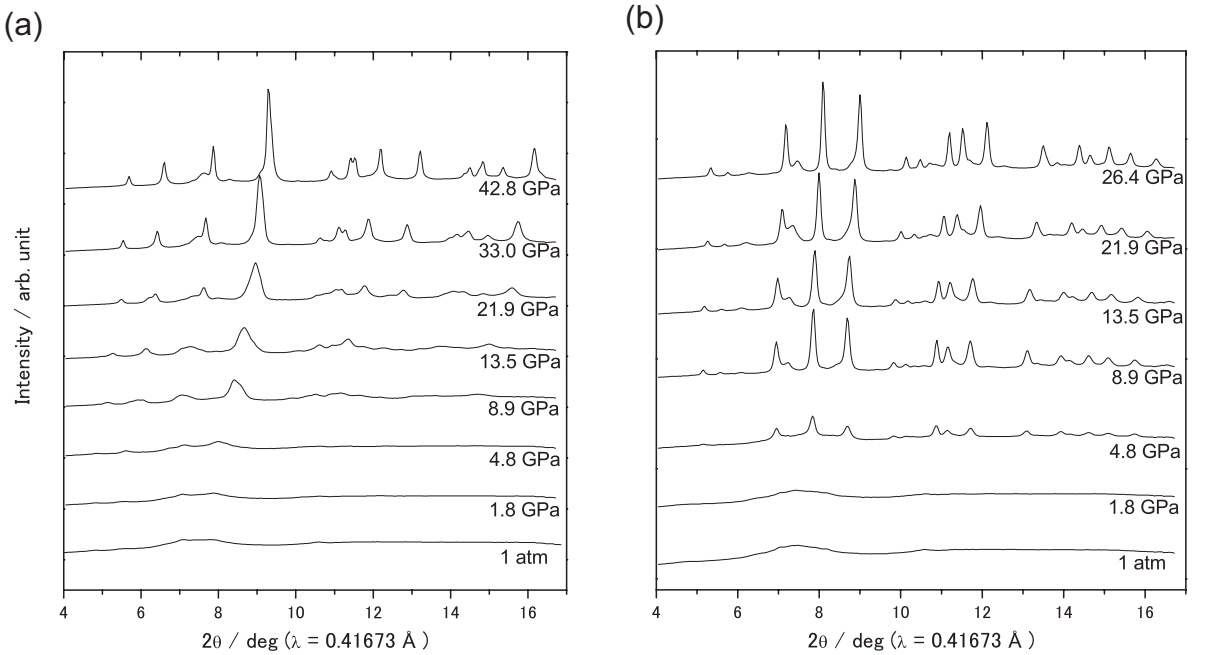

FIGURE 6. Variation of X-ray diffraction patterns under decompression on the 6H (**a**) and 9R perovskites (**b**).

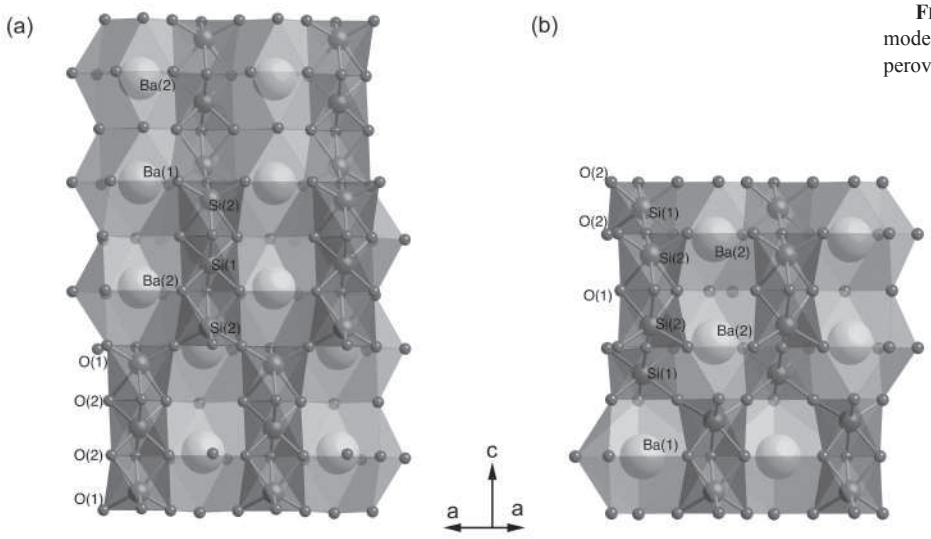

FIGURE 7. Clinographic view of crystal models of 9R (**a**) and 6H (**b**) hexagonal perovskites.

TABLE 7. Interatomic distance of $BaSiO_3$ 6H perovskite at 48.5 GPa

Interatomic distance (Å)		
$Si1O_6$ octahedron		
O2-O2	3.47(4)	×3
O2-O2	2.49(4)	×6
O2-O2	2.41(4)	×6
Si1-O2	1.734(20)	×6
Si1-Si2	3.444(11)	
$Si2O_6$ octahedron		
O1-O2	3.471(30)	×3
O1-O1	2.13(4)	×3
O2-O2	2.62(4)	×3
O1-O2	2.544(21)	×6
Si2-O1	1.805(18)	×3
Si2-O2	1.715(21)	×3
Si2-Si2	2.64(4)	
Ba-O cuboctahedron		
Ba1-O1	2.5682(24)	×6
Ba1-O2	2.568(27)	×6
Ba2-O1	2.579(16)	×3
Ba2-O2	2.5651(21)	×6
Ba2-O2	2.627(27)	×3

that large divalent cations, such as Sr and Ba, are preferentially incorporated into $CaSiO_3$ perovskite rather than $MgSiO_3$ perovskite. Such substitution may yield the face-sharing SiO_6 octahedra locally in $CaSiO_3$ perovskite. Even with a small amount substitution of these large cations, the structural change might induce anisotropy in the perovskite structure, and under the conditions that might be expected in the Earth's lower mantle, this change would then influence the deformation process of perovskite by a dislocation creep (Cordier et al. 2004).

ACKNOWLEDGMENTS

The synchrotron radiation experiments were performed at the BL-10XU in SPring-8 with the approval of the Japan Synchrotron Radiation Research Institute (JASRI) (proposal no. 2005B0285)

REFERENCES CITED

Akimoto, J., Gotoh, Y., and Oosawa, Y. (1994) Refinement of hexagonal $BaTiO_3$. Acta Crystallographica, C50, 160–161.

Angel, R.J. (1997) Transformation of fivefold-coordinated silicon to octahedral silicon in calcium silicate, $CaSi_2O_5$. American Mineralogist, 82, 836–839.

Boullay, Ph., Hervieu, M., Labbe, Ph., and Raveau, B. (1997) Single crystal and HREM study of the "Bi-Sr" stabilized $BaMnO_3$ 9R polytype. Materials Research Bulletin, 32, 35–42.

Chamberland, B.L. (1982) Crystal structure of the 4H $BaCrO_3$ polytype. Journal of Solid State Chemistry, 43, 309–313.

——— (1983) Crystal structure of the 6H $BaCrO_3$ polytype. Journal of Solid State Chemistry, 48, 318–322.

Chamberland, B.L. and Anderson, J.B. (1981) The preparation and crystal structure of a $BaRhO_3$ polytype. Journal of Solid State Chemistry, 39, 114–119.

Cordier, P., Ungar, T., Zsoldos, L., and Tichy, G. (2004) Dislocation creep in $MgSiO_3$ perovskite at conditions of the Earth's uppermost lower mantle. Nature, 428, 837–840.

Glazer, A.M. (1972) The classification of tilted octahedra in perovskites. Acta Crystallographica, B28, 3384–3392.

Grosse, H.P. and Tillmanns, E. (1974a) Bariummetasilicate, $BaSiO_3$(h). Crystal Structure Communications, 3, 603–605.

——— (1974b) Bariumorthosilicate, Ba_2SiO_4. Crystal Structure Communications, 3, 599–602.

Hammersley, A.P. (1997) Fit-2d: in introduction and overview. European Synchrotron Radiation Facility Internal Report ESRF97HA02T.

Hilmer, W. (1962) Die struktur der hochtemperaturform des bariumgermanates $BaGeO_3$(h). Acta Crystallographica, 15, 1101–1105.

Hong, S.-T. and Sleight, A.W. (1997) Crystal structure of 4H $BaRuO_3$: High pressure phase prepared at ambient pressure. Journal of Solid State Chemistry, 128, 251–255.

Horiuchi, H., Ito, E., and Weidner, D.J. (1987) Perovskite-type $MgSiO_3$: Single crystal X-ray diffraction study. American Mineralogist, 72, 357–360.

Kanzaki, M., Stebbins, J.F., and Xue, X. (1991) Characterization of quenched high pressure phases in $CaSiO_3$ system by XRD and ^{29}Si NMR. Geophysical Research Letters, 18, 463–466.

Kato, T., Ringwood, A.E., and Irifune T. (1988) Experimental determination of element partitioning between silicate perovskite, garnet, and liquids: constraints on early differentiation of the mantle. Earth and Planetary Science Letters, 89, 123–145.

Kojitani, H., Kido, M., and Akaogi, M. (2005) Rietveld analysis of a new high-pressure strontium silicate $SrSi_2O_5$. Physics and Chemistry of Minerals, 32, 290–294.

Kubo, A., Suzuki, T., and Akaogi, M (1997) High pressure phase equilibria in the system $CaTiO_3$–$CaSiO_3$: stability of perovskite solid solutions. Physics and Chemistry of Minerals, 24, 488–494.

Larson, A.C. and Von Dreele, R.B. (2004) General Structure Analysis System (GSAS). Los Alamos National Laboratory Report LAUR, 86-748.

Liu, L. and Ringwood, A.E. (1975) Synthesis of perovskite-type polymorph of $CaSiO_3$. Earth and Planetary Science Letters, 28, 209–211.

Longo, J.M. and Kafalas, J.A. (1968) Pressure-induced structural changes in the system $Ba_{1-x}Sr_xRuO_3$. Materials Research Bulletin, 3, 687–692.

Mao, H.K., Xu, J., and Bell, P.M. (1986) Calibration of the ruby pressure gauge to 800 kbar under quasi-hydrostatic conditions. Journal of Geophysical Research, 91, 4673–4676.

Mao, H.K., Chen, L.C., Hemley, R.J., Jephcoat, A.P., Wu, Y., and Bassett, W.A.

(1989) Stability and equation of state of $CaSiO_3$-perovskite to 134 GPa. Journal of Geophysical Research, 94, 17889–17894.

Morishima, H. and Yusa, H. (1998) Numerical calculations of the temperature distribution and the cooling speed in the laser-heated diamond anvil cell. Journal of Applied Physics, 83, 4572–4577.

Ozima, M., Susaki, J., Akimoto, S., and Shimizu, Y. (1982) The system BaO–GeO_2 at high pressure and temperature, with special reference to high-pressure transformation in $BaGeO_3$, $BaGe_2O_5$, and $Ba_2Ge_2O_5$. Journal of Solid State Chemistry, 44, 307–317.

Shim, S.-H., Jeanloz, R., and Duffy, T.S. (2002) Tetragonal structure of $CaSiO_3$ perovskite above 20 GPa. Geophysical Research Letters, 29, 2166 (DOI: 10.1029/2002GL016148).

Shimizu, Y., Syono, Y., and Akimoto, S. (1970) High-pressure transformations in $SrGeO_3$, $SrSiO_3$, $SrGeO_3$, and $BaSiO_3$. High Temperatures and High Pressures, 2, 113–120.

Syono, Y., Akimoto, S., and Kohn, K. (1969) Structure relations of hexagonal perovskite-like compounds ABX_3 at high pressure. Journal of Physical Society of Japan, 26, 993–999.

Watanuki, T., Shimomura, O., Yagi, T., Kondo, T., and Isshiki, M. (2001) Construction of laser-heated diamond anvil cell system for in-situ X-ray diffraction study at SPring-8. Review of Scientific Instruments, 72, 1289–1292.

Yusa, H., Akaogi, M., Sata, N., Kojitani, H., Kato, Y., and Ohishi, Y. (2005) Unquenchable hexagonal perovskite in high-pressure polymorphs of storontium silicates. American Mineralogist, 90, 1017–1020.

Manuscript received May 19, 2006
Manuscript accepted October 30, 2006
Manuscript handled by Guoyin Shen